JOURNAL OF AIRCRAFT
Vol. 31, No. 3, May–June 1994

Unstructured Mesh Quality Assessment and Upwind Euler Solution Algorithm Validation

Paul R. Woodard*
Purdue University, West Lafayette, Indiana 47907
John T. Batina†
NASA Langley Research Center, Hampton, Virginia 23681
and
Henry T. Y. Yang‡
Purdue University, West Lafayette, Indiana 47907

Quality assessment procedures are described for two- and three-dimensional unstructured meshes. The procedures include measurement of minimum angles, element aspect ratios, stretching, and element skewness. Meshes about the ONERA M6 wing and the Boeing 747 transport configuration are generated using an advancing front method grid generation package of programs. Solutions of the Euler equations for these meshes are obtained at low angle-of-attack, transonic conditions. Results for these cases, obtained as part of a validation study, investigate accuracy of an implicit upwind Euler solution algorithm.

Introduction

In recent years, considerable progress has been made in developing computational fluid dynamics (CFD) methods for unstructured triangular and tetrahedral meshes.[1–9] These meshes are an alternative to the traditional structured meshes, for which many CFD algorithms have been developed. Unstructured meshes have several distinct advantages over their structured mesh counterparts. For example, they can treat arbitrary complex geometries effectively, and they readily lend themselves to spatial adaption procedures. These advantages result from the arbitrary nature of the numbering and placement of the nodes and elements which make up a mesh.

The generation of unstructured meshes generally falls into three broad categories: 1) the triangularization of structured grids, 2) Voronoi/Delaunay triangularization,[10–16] and 3) the advancing front method.[4,17–20] However, regardless of what method was used to generate the unstructured mesh, the quality of these meshes oftentimes is not acceptable for flow solution. With meshes for realistic three-dimensional configurations having a quarter million or more elements, the computer time required to solve the flow equations on one of these meshes is relatively large. Because problems in these meshes can significantly affect the solution time and accuracy, it becomes important to be able to assess the quality of a mesh before many hours of computer time are used in an attempt to obtain a solution on a mesh of questionable quality. A summary, e.g., of some mesh quality measures is given by Baker,[14,15] and a strategy for improving mesh quality is described by Formaggia.[17]

Presented as Paper 92-0444 at the AIAA 30th Aerospace Sciences Meeting, Reno, NV, Jan. 6–9, 1992; received March 10, 1992; revision received May 27, 1993; accepted for publication May 27, 1993.

*Graduate Research Assistant, School of Aeronautics and Astronautics. Member AIAA.
†Senior Research Scientist, Unsteady Aerodynamics Branch, Structural Dynamics Division. Associate Fellow AIAA.
‡Professor and Dean, Schools of Engineering. Fellow AIAA.

To assess the state of unstructured mesh grid generation, an advancing front method grid generation package of programs was used in the present study,[19] and several measures were created to determine and assess mesh quality. Meshes were generated about the ONERA M6 wing and about the Boeing 747 transport configuration. The purpose of this article is to report the quality evaluations that were performed for these meshes and to present numerical solutions of the Euler equations that are determined on these meshes. Steady flow results are calculated on these meshes and are compared to experimental data as part of a validation study of a three-dimensional implicit upwind Euler solution algorithm.

Advancing Front Method

In the two-dimensional advancing front method, elements are generated by marching a "front" of free sides into the computational domain. The initial front is created by subdividing the prescribed boundary segments according to the spacing determined by interpolation from a background grid, an example of which is shown in Fig. 1a. New triangles are created by extending this front, also according to the background spacing. If possible, an existing node is used to generate this new element, but, if necessary, a new node is created. Once a new element has been created, the front is updated to reflect changes due to the creation of the new element, as shown in Fig. 1b. This procedure continues until all sides in the front are removed, and the domain is meshed, as shown in Fig. 1c.

The method works similarly in three dimensions. The initial front is composed of a surface mesh of triangles. This surface mesh is created by applying the two-dimensional grid generator to surface regions which are specified by taking convenient subsets of the entire boundary. These regions first must be mapped to a two-dimensional computational space,

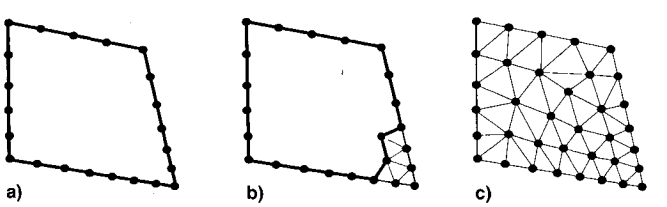

Fig. 1 Advancing front method: a) initial front, b) advancing the front, and c) the final mesh.

then back to three dimensions once a region is meshed. From this front, a triangular side is chosen to create a new element. A new tetrahedron is formed, using either a new or an existing node. The front then is updated, and the process continues until the entire region is meshed.

When generating a three-dimensional mesh, care must be taken to insure that the surface normals from each region point into the computational domain. Another potential difficulty occurs if the background mesh does not cover the entire flowfield domain. In this case, errors are produced when the front reaches the area not covered by the background grid. This especially can happen if there are holes in the background grid or if somehow it is turned inside out.

VGRID3D

The VGRID3D package of programs, provided by Parikh and Pirzadeh,[19] consists basically of one core program; however there are several pre- and postprocessing programs as well. Among them is a program to input the surface data, graphically taken from existing structured data. Another preprocessing program is used to input data graphically and to make modifications to the background mesh. This program treats three line types, including straight lines, parabolic lines, and arbitrary splined lines. There also are five kinds of surfaces, including planar, three and four segment parabolic, and three and four segment arbitrary surfaces. Using these different surfaces, it is possible to define arbitrary geometries.

The VGRID3D program maps the surface information to and from computational space by solving the Poisson equation based on the boundary segments. For this reason, "small" surface regions must be used in VGRID3D so that the interior geometry is not adversely affected. Also, the data structure utilized by VGRID3D makes it conducive to taking information from a pre-existing data file, such as might be output by a CAD/CAM package, and easily converting it, using one of the preprocessing programs.

The greatest advantage of the VGRID3D program is the graphical interface. Written to run on a Silicon Graphics Iris Workstation, the program is able to display the surface mesh quickly from a variety of different locations, as well as being able to plot the front itself as it advances. In this way, the user can view the mesh as it is being created. There are also disadvantages. One disadvantage is that the input data is not modified easily. Adding elements to an existing data structure can require significant work. Because all nonplanar surfaces must have either three or four segments as their boundaries, the addition of new components, such as stores or flaps, can increase greatly the number of surfaces, segments, and points required, not to mention the increased complexity of the data file itself.

Two-Dimensional Grid Quality

Grid qualities were defined first for two-dimensional meshes before investigating the quality of three-dimensional meshes. These two-dimensional qualities are described here briefly for simplicity. A complete set of two-dimensional mesh quality results may be found in Ref. 21.

Many quality measures can be devised for two-dimensional grids,[14,15] but they generally all fall into two categories, individual element quantities and local or global mesh quantities. Individual element quantities are those which apply to elements by themselves, regardless of the surrounding mesh. Local quantities are those which apply to how an individual element "fits in" with the elements which surround it. These can be applied as local measures, if taken near an airfoil or other area of interest, or as global measures if taken over the entire mesh. One reason the parameters described below are chosen as two-dimensional quality measures is that they all can be extended readily to three dimensions.

Individual Element Quality

It is generally accepted that a mesh composed of equilateral triangles is ideal for two-dimensional unstructured meshes, just as a mesh composed of squares is ideal for structured meshes. Among individual element quantities, one that is in common use is a measure of the minimum angle of a triangle. By maximizing the minimum angle, an element becomes more uniform. By making use of the vector dot product, this quantity is reasonably simple to compute. It is not, however, the only measure of element quality.

A far less sophisticated method is to take the ratio of the maximum and minimum side lengths for each element. This is shown graphically in Fig. 2a. This puts a bound on the minimum angle, but it requires less computation. In general, the extra computation required to determine the minimum angle itself is small. When these concepts are extrapolated to three-dimensions, however, small savings in individual computations can become significant.

Another way to measure element quality, shown in Fig. 2b, is to define an aspect ratio for each element. This is defined by taking the ratio of the area of the smallest circle that can be superscribed about the triangle to the area of the largest circle that can be inscribed within the triangle. This measure then is normalized using the aspect ratio of an equilateral triangle, strictly for the sake of convenience, so that an aspect ratio of 1 indicates an equilateral triangle.

Local Mesh Quality

To measure local mesh qualities, information must be known about the neighboring elements. Because of the inherent random nature of unstructured grids, neighboring element information must also be known, resulting in additional computational overhead. At the very minimum, the identity of the three triangles which surround a given triangle must be known. Additional nodal and connectivity information also are computed and stored for convenience.

Any of the above individual element quality measures also can be used as local mesh quality measures by taking ratios of their values across sides. For example, it might be advantageous to compare the aspect ratio of elements across edges. While these adapted measures can be useful, there are other local mesh quality measures which do not have individual element analogies. The most common of these is area ratios. These area ratios are useful to determine the amount of stretching in the mesh. For internal flow problems, such as ducts, this is not a great problem, but for external flows, such as airfoils, the stretching can be significant.

Another local quality measure is element skewness. A triangle can be formed using the midpoint of the side of interest and the two opposing vertices as shown in Fig. 3. The area of this triangle divided by the average area of the two base

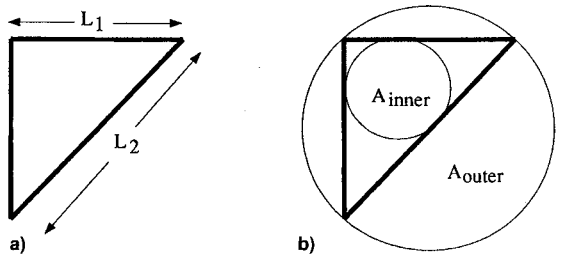

Fig. 2 Definition of individual element quality parameters: a) length ratio and b) aspect ratio.

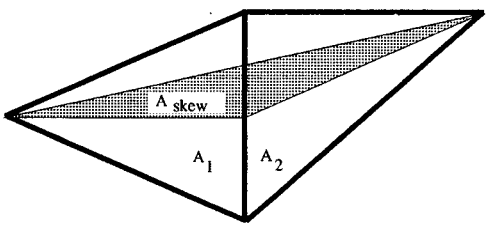

Fig. 3 Area ratio and skewness definitions.

triangles gives the skewness across that face. This parameter is 0 for a well-aligned mesh and, in general, will be less than 1, except for highly-distorted meshes.

Three-Dimensional Grid Quality

The following subsections address individual element quality and local mesh quality as they apply to three-dimensional grids. Similar quality measures have been reported previously by Baker[14-16] and Formaggia.[17]

Individual Element Quality

In three-dimensional meshes, the minimum angle measurement becomes the minimum dihedral angle measurement. The dihedral angle is measured using the vector dot product for each combination of the four faces which make up the tetrahedron. From this, the minimum of the six dihedral angles is found.

Another way to measure element quality is to take a ratio of the areas of the largest and smallest faces. The areas are found by taking the vector cross product of two of the three edges which make up a face. The magnitude of this vector is used as the area. This is far less computationally intensive than computing the dihedral angles for each face, and yields similar results.

An aspect ratio for a tetrahedron can be defined as the ratio of the volume of the smallest sphere that can surround the tetrahedron to the volume of the largest sphere that can be fit within the tetrahedron. This ratio then is normalized by the value of a "regular" tetrahedron with equilateral faces.

There are other computations which can be made easily at the same time as other quality measures. One is an orientation checker. If the right-hand rule is applied to all the faces in a tetrahedron, two faces will have normals which point inward, and two will have faces that point outward. Normally, the connectivity information for these nodes is random, so checks must be made by the flow solver to determine which faces point inward and which point outward. If, however, all the nodes are arranged with the fourth node "on top" of the first three, then the faces opposite the first and fourth nodes always will point inward, and the faces opposite the second and third nodes will point outward.

Local Mesh Quality

There also are local mesh quantities for three-dimensional meshes. These also require some information about the neighboring elements. As a minimum, the element numbers for the four neighbor elements must be known. If possible, it is beneficial to also store additional information, such as the neighboring element orientation or neighboring nodes. Also, as the two-dimensional quantities are measured across sides, the three-dimensional ones are measured across faces. Variations of the above individual element quantities can be measured across element faces, yielding some local quality measures.

In three dimensions, volume ratios are useful measures of stretching, just as area ratios are important in two dimensions. Mesh stretching is even more important in three dimensions than it is in two. This is because a doubling in the linear spacing will result in an eightfold increase in volume, and, consequently, large changes in the volume ratios are likely. These changes can be located with the volume parameter, indicating problems in the background grid.

Skewness measures also can be computed for three-dimensional elements. Using the two nodes on the opposite sides of the face of interest and the center of the face, a triangle is formed. The area of this triangle divided by the area of the face itself becomes the skewness. For two ideally aligned elements, the area of the formed triangle will be zero, resulting in zero skewness.

There are other problems with meshes in three dimensions which may be detected during quality assessment. One such problem with tetrahedral meshes is that it is difficult to find elements with negative volume. These can occur after smoothing has been applied, or perhaps even by the grid generation program itself. One way to find these elements is to perform a global volume check. The absolute value of the volume of each of the elements is summed and compared to the expected volume enclosed by the boundaries. The problem with this method is that except for meshes with strictly defined outer boundaries, the expected volume is extremely difficult to compute. Even assuming it is calculable, the errors introduced potentially are greater than the volume of the element with negative area itself. Another problem with this method is that even if it works, it will only confirm the existence of a negative volume element. It is still up to the user to find that element. However, by comparing nodes across faces, it is possible not only to locate the presence of elements with negative volumes quickly and accurately, but to identify the elements themselves. For two adjoining elements with positive volume, their off nodes will be on opposite sides of the common face. For a combination of two elements, one of which has positive volume and the other which is distorted, these nodes will be on the same side of the common face. For a distorted mesh with two adjoining elements with negative volumes, this test will fail for this face but will pass for other faces of the distorted tetrahedron.

Solution Algorithm

The inviscid flow about several unstructured two- and three-dimensional meshes was determined by solving the time-dependent Euler equations. The computational method is an implicit upwind flow solver that uses Roe's flux-difference splitting. The implicit temporal discretization is a two-sweep Gauss-Seidel relaxation procedure that is computationally efficient for either steady or unsteady flow problems. Details about the solution algorithm are given by Batina.[22,23]

Results

Calculations were performed to determine the quality of several unstructured meshes and to assess the accuracy of the flow solver by comparing calculations with experimental data. Three-dimensional results were obtained for two configurations for a variety of meshes and different flow conditions. An ONERA M6 wing[24] case was studied for a freestream Mach number M_∞ of 0.84 and an angle-of-attack α of 3.06 deg, which is hereafter referred to as case 1. Additionally, meshes were generated about the Boeing 747 transport configuration, and a set of calculations were made. This is at $M_\infty = 0.70$ and $\alpha = 2.72$ deg which is referred to as case 2.

ONERA M6 Wing

To investigate spatial accuracy, results were obtained on three ONERA M6 wing meshes. This wing has been widely studied, and results have been obtained using many other flow solvers, on both structured and unstructured meshes. The wing has a leading-edge sweep of 30 deg, an aspect ratio of 3.8, and a taper ratio of 0.56. It has a symmetrical cross section, a root chord of 0.6775, a semispan of 1.0, and a rounded tip. For this configuration, three meshes, the surface triangularizations of which are shown in Fig. 4, were generated. Sizes of these meshes are summarized in Table 1. These meshes are of increasing grid density to investigate the effects of mesh spacing on the calculated solution. Nodes are placed

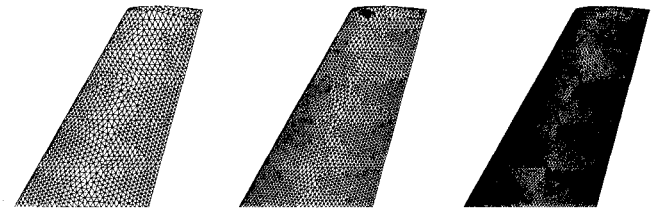

Fig. 4 Surface triangularization for ONERA M6 wing meshes.

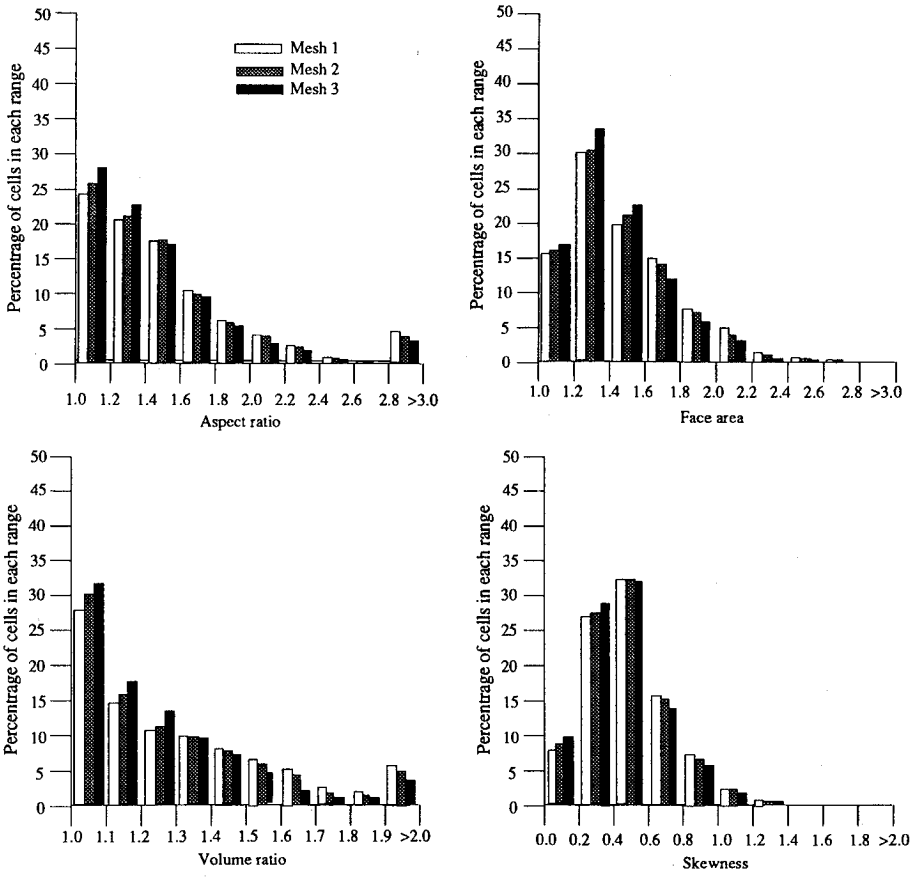

Fig. 5 Comparison of mesh qualities for three ONERA M6 wing meshes.

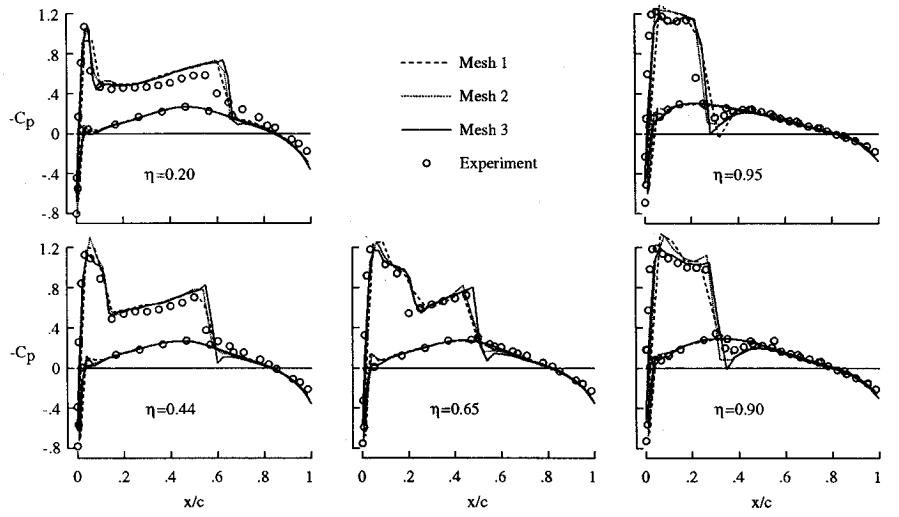

Fig. 6 Comparison of calculated and measured coefficients of pressure on the ONERA M6 wing at $M_\infty = 0.84$ and $\alpha = 3.06$ deg.

Table 1 Comparisons of ONERA M6 wing meshes

	Mesh 1	Mesh 2	Mesh 3
Number of cells	47,344	98,317	288,170
Number of nodes	9,401	19,048	53,989
Number of boundary faces	5,860	10,388	23,164
Number of boundary nodes	2,932	5,196	11,584

Table 2 Convergence characteristics for ONERA M6 wing meshes for case 1

	Mesh 1	Mesh 2	Mesh 3
CPU time (Cray-2 min)	18	52	494
Iterations	998	1328	3258

on these three meshes along the chord at the span stations $\eta = 0.2, 0.44, 0.6, 0.8, 0.9$, and 0.95 to aid in making comparisons with the experimental pressure data of Ref. 24.

Mesh qualities for the ONERA M6 wing meshes are shown in Fig. 5. These assessment plots show the percentage of cells in each mesh which fall into certain quality ranges. For a uniform mesh of regular tetrahedra, 100% of the cells would be in the leftmost columns. All three meshes were generated using the same mesh input data and background grid, with the only differences being in the global spacing parameter. Therefore, it is not unexpected that the three meshes are of similar quality. It is worth noting that mesh quality improves as the mesh density increases, suggesting that increases in grid density lead to more uniform cells.

At the present time, the mesh quality procedures can do little more than serve as a test to show if a mesh is or is not

Table 3 Force and moment coefficients for ONERA M6 wing meshes

	Mesh 1	Mesh 2	Mesh 3	Ref. 8
Lift coefficient	0.2892	0.2893	0.2923	0.2911
Drag coefficient	0.0195	0.0167	0.0140	0.0123
Moment coefficient	−0.1715	−0.1702	−0.1717	−0.1726

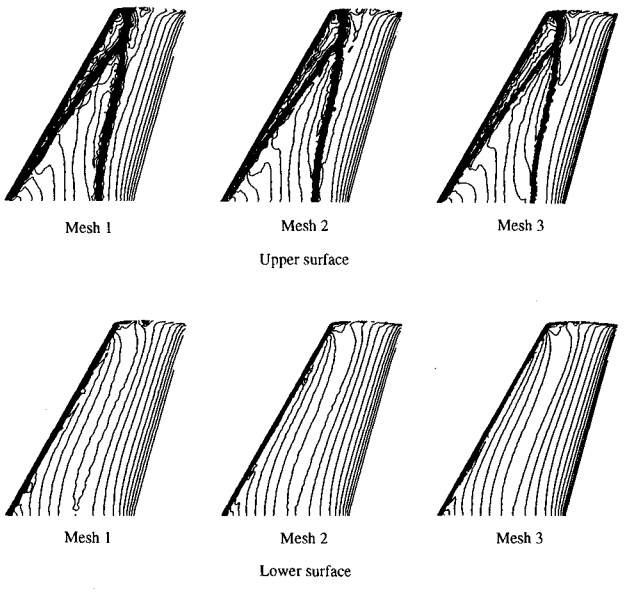

Fig. 7 Surface pressure contours on the ONERA M6 wing for three meshes at $M_\infty = 0.84$ and $\alpha = 3.06$ deg ($\Delta P/P_\infty = 0.02$).

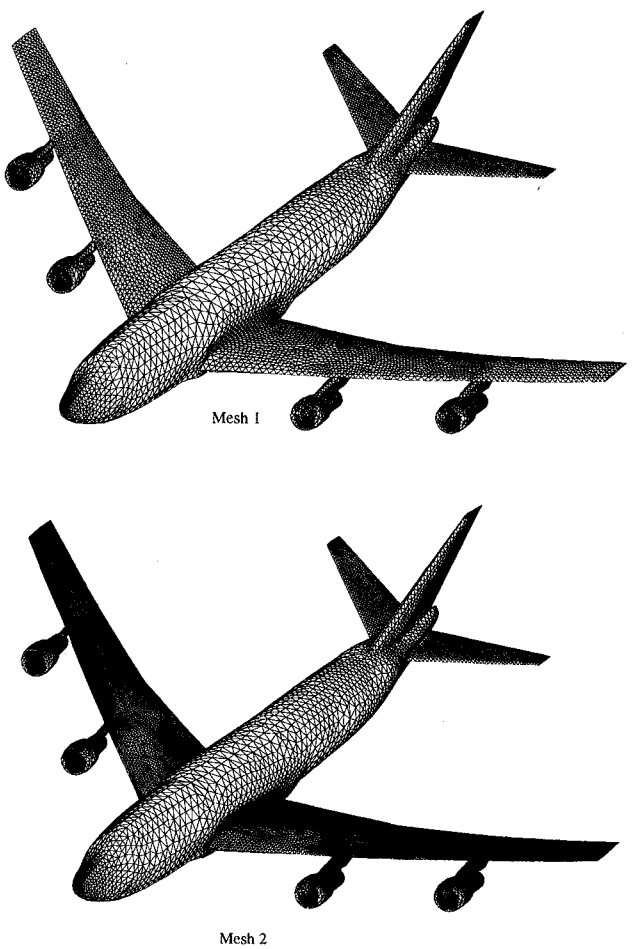

Fig. 8 Surface triangularization of two Boeing 747 transport configuration meshes.

Table 4 Comparisons of Boeing 747 transport configuration meshes

	Mesh 1	Mesh 2
Number of cells	216,864	441,731
Number of nodes	39,847	80,520
Number of boundary faces	14,254	26,423
Number of boundary nodes	7,121	13,208

suitable for use. It is possible to use these techniques to isolate a given poorly shaped cell, or region of cells; however, the remeshing of this region can be tedious especially if the region contains a large number of cells. In general, the practical option is to remesh the entire domain, after altering the background mesh in the regions of difficulty.

Convergence information for case 1 is shown in Table 2. This table shows the time required to achieve a four order of magnitude reduction in the L_2-norm of the density residual, which was selected as the level for acceptable convergence. For mesh 1, a converged solution was obtained in about 18 min of Cray-2 CPU time. For mesh 2, a converged solution was obtained in less than 1 h of CPU time, while a solution on mesh 3 required about 8 h. Coefficients of pressure are shown in Fig. 6. In these plots, coefficients of pressure computed using mesh 1 are denoted by the dashed lines, coefficients of pressure on mesh 2 are given by the dotted line, coefficients of pressure on mesh 3 are given by the solid line, and experimental data is represented by the circles. For this case, a double shock wave occurs on the upper surface of the wing and coalesces into a single, relatively strong shock near the wingtip. As expected, coefficients of pressure for mesh 3 show the sharpest resolution of the double shock wave. Results for all three meshes show good agreement with each other aft of the 70% chord line on the upper surface, and aft of the 25% chord line on the lower surface. Pressure contours for this case are shown in Fig. 7 for the three meshes. The contours on all three meshes show the double shock wave on the upper surface. The contours on mesh 3 show much sharper shock waves than the other two meshes, demonstrating an effect of mesh density. On the lower surface, there is less of a noticeable difference between the three sets of results.

Coefficients of lift, drag, and pitching moment about the wing apex are given for the three meshes in Table 3. These values were obtained by summing face centered values around the wing. Additionally, the table presents lift, drag, and moment values reported in Ref. 8 which were computed on a mesh with 231,507 elements and 16,984 nodes. This demonstrates good agreement between the present method and another unstructured upwind Euler solver.

Boeing 747 Transport

To investigate a more complex configuration, the Boeing 747 transport configuration was chosen. In addition to the wing and fuselage, this configuration includes flow-through engine nacelles and horizontal and vertical tails. Two meshes were generated for this configuration, the surface triangularizations of which are shown in Fig. 8. For these meshes, the same surface input data was used, but different background grids were applied to achieve different density.

Mesh 1 is relatively coarse, with no dramatic increase in mesh spacing along the wing. Mesh 2 is considerably finer, especially near the wing leading edge. Table 4 presents a summary of the mesh sizes. Mesh qualities are given for the two meshes in Fig. 9. Based on the quality evaluations, mesh

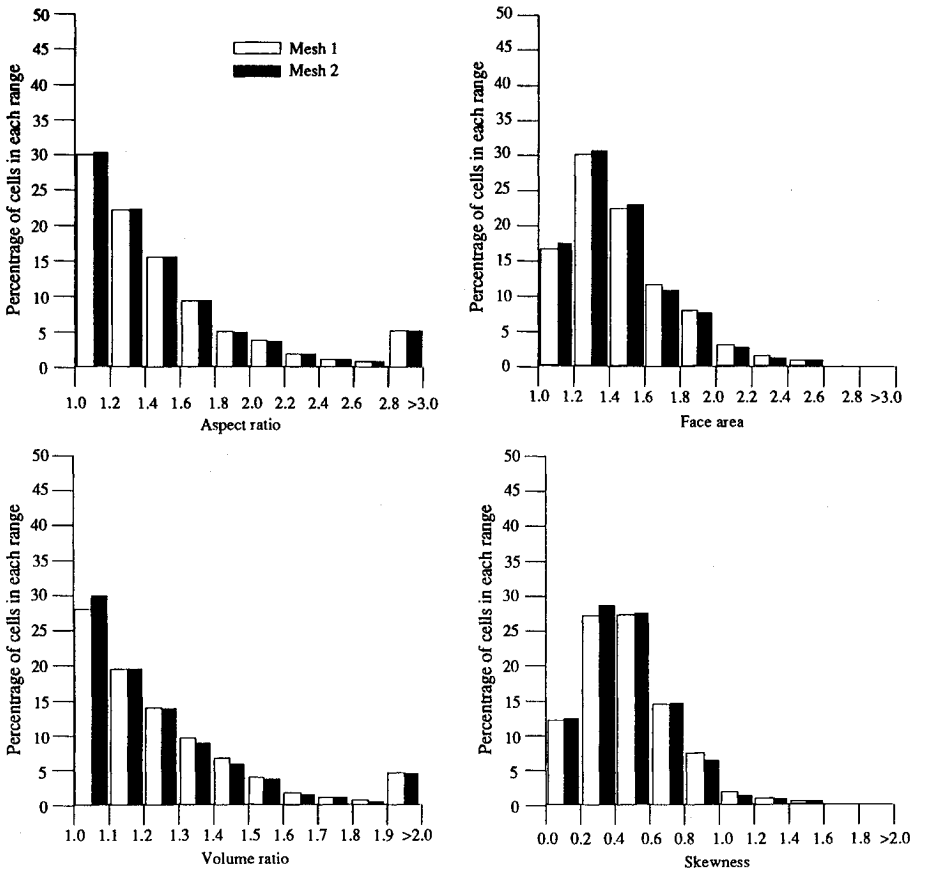

Fig. 9 Comparison of mesh quality for two Boeing 747 transport configuration meshes.

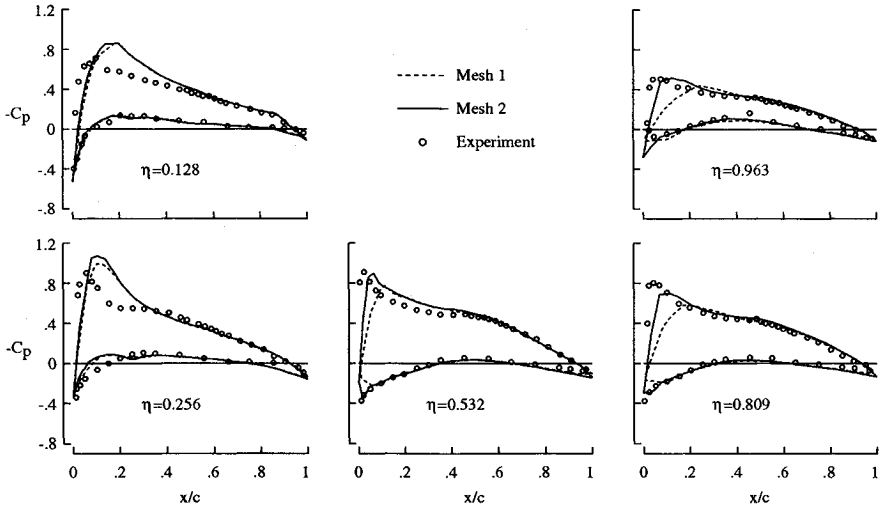

Fig. 10 Comparison of calculated and measured coefficients of pressure on the Boeing 747 transport configuration at $M_\infty = 0.7$ and $\alpha = 2.72$ deg.

2 is of slightly higher quality, which is expected due to the decrease in mesh spacing.

Convergence information for case 2 is shown in Table 5. Mesh 1 required about 4.5 h of Cray-2 CPU time, and the calculation on Mesh 2 was converged in slightly over 12 h. Coefficients of pressure for case 2 on the wing at several span stations are shown in Fig. 10, along with experimental data. Values for mesh 1 are given by the dashed lines, values for mesh 2 are given by the solid lines, and experimental data is represented by the circles. Calculations for mesh 2 show good agreement with experimental data, especially at the outer span stations. The differences between the two sets of calculations are primarily due to the differences in mesh density near the wing leading edge. Further refinement of the mesh near the leading edge should result in better agreement with experimental pressures. Lower surface comparisons with experiment are very good along the entire span, and differences along the upper surface at the inboard span stations are believed to be the result of a combination of factors, including viscous effects, and possible inaccuracies in the modeling of the wing/fuselage junction region. Pressure contours about the entire aircraft for mesh 2 are shown in Fig. 11. Flow expansion occurs along the upper surface of the wing, the horizontal tail, and the nose region of the fuselage. Stagnation occurs near the wing and tail leading edges, and the front of the engine nacelles. Also the effect of interference between the wing and the fuselage is indicated by the contour lines that wrap around the fuselage beginning just aft of the leading edge of the wing. This demonstrates the ability of the solution algorithm to effectively treat a complex configuration.

Table 5 Convergence characteristics for Boeing 747 transport configuration meshes for case 2

	Mesh 1	Mesh 2
CPU time (Cray-2 min)	268	732
Iterations	1690	2237

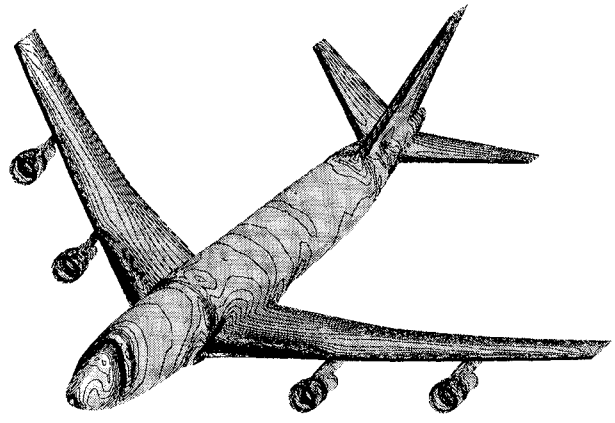

Fig. 11 Pressure contours on a Boeing 747 transport configuration computed using mesh 2 at $M_\infty = 0.7$ and $\alpha = 2.72$ deg.

Concluding Remarks

Quality assessment procedures were described for two- and three-dimensional unstructured meshes. The procedures include measurement of minimum angles, element aspect ratios, stretching, and element skewness. Meshes about the ONERA M6 wing and the Boeing 747 transport configuration were generated using an advancing front method grid generation package, and qualities of these meshes were assessed.

Validation of an implicit upwind Euler solution algorithm was begun by obtaining solutions of the Euler equations for these meshes at low angle of attack, transonic conditions. Results for these cases demonstrated the accuracy of the current solution algorithm. Comparisons of calculated pressures with experimental data show excellent agreement for the ONERA M6 wing meshes. Similar comparisons of calculated pressures with experimental data for the 747 configuration also show favorable agreement.

Acknowledgments

The work constitutes a part of the first author's M.S. Thesis at Purdue University and was supported by the NASA Langley Graduate Aeronautics Program under Grant NAG-1-372. The authors acknowledge Paresh Parikh and Shahyar Pirzadeh of ViGYAN Inc., Hampton, Virginia, and Neal Frink of the Transonic Aerodynamics Branch at NASA Langley Research Center, Hampton, Virginia, for providing the VGRID3D software which was used to create the meshes in the present study.

References

[1]Jameson, A., Baker, T. J., and Weatherill, N. P., "Calculation of Inviscid Transonic Flow over a Complete Aircraft," AIAA Paper 86-0103, Jan. 1986.

[2]Mavriplis, D., and Jameson, A., "Multigrid Solution of the Two-Dimensional Euler Equations on Unstructured Triangular Meshes," AIAA Paper 87-0353, Jan. 1987.

[3]Rausch, R. D., Batina, J. T., and Yang, H. T. Y., "Euler Flutter Analysis of Airfoils Using Unstructured Dynamic Meshes," AIAA Paper 89-1384, April 1989.

[4]Peraire, J., Morgan, K., and Peiro, J., "Unstructured Finite Element Mesh Generation and Adaptive Procedures for CFD," AGARD-CP-464, May 1989.

[5]Batina, J. T., "Accuracy of Unstructured-Grid Upwind-Euler Algorithm for the ONERA M6 Wing," Accuracy of Unstructured Grid Techniques Workshop, NASA Langley Research Center, Hampton, VA, Jan. 1990.

[6]Kleb, W. L., Batina, J. T., and Williams, M. H., "Temporal Adaptive Euler/Navier-Stokes Algorithm for Unsteady Aerodynamic Analysis of Airfoils Using Unstructured Dynamic Meshes," AIAA Paper 90-1650, June 1990.

[7]Rausch, R. D., Batina, J. T., and Yang, H. T. Y., "Spatial Adaption Procedures on Unstructured Meshes for Accurate Unsteady Aerodynamic Flow Computation," AIAA Paper 91-1106, April 1991.

[8]Frink, N. T., Parikh, P., and Pirzadeh, S., "A Fast Upwind Solver for the Euler Equations on Three-Dimensional Unstructured Meshes," AIAA Paper 91-0102, Jan. 1991.

[9]Frink, N. T., Parikh, P., and Pirzadeh, S., "Aerodynamic Analysis of Complex Configurations Using Unstructured Grids," AIAA Paper 91-3292, Sept. 1991.

[10]Watson, D. F., "Computing the N-Dimensional Delaunay Tesselation with Application to Voronoi Polytopes," *The Computer Journal*, Vol. 24, No. 2, 1981, pp. 167–172.

[11]Sloan, S. W., and Houlsby, G. T., "An Implementation of Watson's Algorithm for Computing 2-Dimensional Delaunay Triangulations," *Advanced Engineering Software*, Vol. 6, No. 4, 1984, pp. 192–197.

[12]Tanemura, M., Ogawa, T., and Ogita, N., "A New Algorithm for Three-Dimensional Voronoi Tesselation," *Journal of Computational Physics*, Vol. 51, 1983, pp. 191–207.

[13]Baker, T. J., "Three-Dimensional Mesh Generation by Triangulation of Arbitrary Point Sets," AIAA Paper 87-1124, June 1987.

[14]Baker, T., "Automatic Mesh Generation for Complex Three-Dimensional Regions Using a Constrained Delaunay Triangulation," *Engineering with Computers*, Vol. 5, 1989, pp. 161–175.

[15]Baker, T., "Unstructured Meshes and Surface Fidelity for Complex Shapes," AIAA Paper 91-1591, June 1991.

[16]Baker, T. J., "Element Quality in Tetrahedral Meshes," *Proceedings of the 7th International Conference on Finite Element Methods in Flow Problems* (Huntsville, AL), April 1989, pp. 1018–1024.

[17]Formaggia, L., "An Unstructured Mesh Generation Algorithm for Three Dimensional Aeronautical Configurations," *Proceedings of the 3rd International Conference of Numerical Grid Generation in Computational Fluid Dynamics* (Edited Arcilla) (Barcelona, Spain), June 1991, pp. 249–260.

[18]Lohner, R., and Parikh, P., "Generation of Three-Dimensional Unstructured Grids by the Advancing Front Method," *International Journal of Numerical Methods in Fluids*, Vol. 8, 1988, pp. 1135–1149.

[19]Parikh, P., Pirzadeh, S., and Lohner, R., "A Package for 3-D Unstructured Grid Generation, Finite-Element Flow Solution and Flow Field Visualization," NASA CR-182090, Sept. 1990.

[20]Pirzadeh, S., "Recent Progress in Unstructured Grid Generation," AIAA Paper 92-0445, Jan. 1992.

[21]Woodard, P. R., "Grid Quality Assessment for Unstructured Triangular and Tetrahedral Meshes and Validation of an Upwind Implicit Euler Solution Algorithm," M.S. Thesis, Purdue University, West Lafayette, IN, May 1992.

[22]Batina, J. T., "A Fast Implicit Upwind Solution Algorithm for Three Dimensional Unstructured Dynamic Meshes," AIAA Paper 92-0447, Jan. 1992.

[23]Batina, J. T., "Implicit Upwind-Euler Solution Algorithms for Unstructured-Grid Applications," First European Computational Fluid Dynamics Conference, Brussels, Belgium, Sept. 1992.

[24]Schmidt, V., and Charpin, F., "Pressure Distributions on the ONERA M6 Wing at Transonic Mach Numbers," *Experimental Data Base for Computer Program Assessment*, Appendix B1 in AGARD-AR-138, May 1979.